International Journal of Scientific Research in Physics and Applied Sciences
Vol.10, Issue.3, pp.01-14, June (2022)

Research Paper

E-ISSN: 2348-3423

Studies of Structural, Optical and Electrical Properties of Pure and l-ornithine Monohydrochloride Doped KDP Crystals

H. Bhuva[1*], K.V. Vadhel[2], M.J. Joshi[3], H.O. Jethva[4]

[1,2,3,4]Department of Physics, Saurashtra University, Rajkot, Gujarat, India

[*]*Corresponding Author: harshalbhuva77@gmail.com*

Available online at: www.isroset.org | DOI: https://doi.org/10.26438/ijsrpas/v10i3.114

Received: 18/Apr/2022, Accepted: 20/May/2022, Online: 30/Jun/2022

***Abstract*—** In the current study, author examines and reports the effect of dopant l-ornithine monohydrochloride (LOMHC) on structural, optical and electrical properties of potassium dihydrogen phosphate (KDP) crystal. The slow solvent evaporation technique is used to grow the crystals. Good grade, transparent, and rectangular crystals are achieved after approximately 4 weeks. The grown crystals are characterized by powder X, SHG, UV-Vis, impedance, modulus, dielectric and conductivity analysis. The powder X analysis shows single phase nature of the doped crystals with increase in crystallite size and lattice strain. The doped KDP crystals show NLO behavior with reduction in SHG efficiency. The UV-Vis analysis shows reduction in transmittance % and band gap energy of doped KDP crystals. Complex impedance and modulus analysis show the dominancy in polarization mechanism in all the samples due to bulk effect arising in the grains. The scaling behavior of modulus demonstrates the reliance of relaxation dynamics on doped LOMHC concentration. The dielectric behavior of pure and LOMHC doped KDP shows normal behavior. The ac conductivity obeys the Jonscher's power law and ideal long-range pathways and diffusion limited hopping process in pure and LOMHC doped KDP crystals.

***Keywords*—** KDP, Powder XRD, SHG, UV-Vis, electrical analysis

I. INTRODUCTION

KDP is a very useful single crystal due to its capability of frequency conversion [1,2]. The small amount of different types of impurities can influence the rate of growth, shape and transparency of growing pure crystals as well as upswing optical-electrical characteristics. Parikh et al. and N. Kanagathara [3,4] have studied l-lysine doped KDP crystals and reported increased %transmittance and SHG efficiency and decreased dielectric constant and loss value. Ravi et al. [5] have studied phenylalanine doped KDP reported increased SHG efficiency of doped KDP crystals. Rajesh et al. [6] have studied equi-molar l-serine KDP crystal and reported increased SHG efficiency of the crystal compared to KDP. O V Mary Sheeja [7] reported CdS nanoparticles doped KDP crystals and reported increased % of optical transmission and SHG efficiency. Metals, such as mercury and silver doped KDP crystals have been reported by Mayilvani [8] and observed increased transmittance of mercury doped KDP, while lower transmittance of silver doped KDP. So on, the study of doped KDP crystal is much necessary in order to find out the appropriate dopant and its concentration for which the optical and electrical properties are improved or not. With this aim, the present authors decide to investigate the influence of l-ornithine monohydrochloride (LOMHC) doping by varying its weight% on the structural, optical and electrical properties of pure KDP crystals. Further, it is worth to mention here that as LOMHC is a polyamino acid, its carboxyl and amino group no longer able to act as acid or base but the acid base property depends upon the overall ionization characteristics of the side chain methylene (CH2) and amino (NH2) group. It is expected that the same should be reflected in terms of either increase or decrease in SHG efficiency of LOMHC doped KDP crystals.

II. EXPERIMENTAL TECHNIQUE

Slow solvent evaporation is utilised to grow pure and LOMHC doped KDP crystals at room temperature. In 500 ml of distilled water, KDP is added accordingly till the solution is enriched. Also, the stirring process is done to acquire homogeneity. After filtering, the whole solution is separated into 5 beakers of 100 ml each. One beaker is used to grow only KDP crystal and 0.2gm, 0.4gm, 0.6gm, and 0.8gm LOMHC is dissolved with proper stirring to grow 0.2, 0.4, 0.6, and 0.8 weight% LOMHCl doped KDP crystals in other beakers, respectively. For controlled evaporation, all beakers are stored in a dust-free and disturbance-free environment and coated with filter paper. Good grade, transparent, rectangular crystals are meticulously extracted from the beakers after 4 weeks. Figure 1a-e shows pure and LOMHC doped KDP crystals. As can be seen in Figure 1, all of the crystals possess

almost rectangular shape morphology and transparency of which decreases as wt% of dopant LOMHC increases.

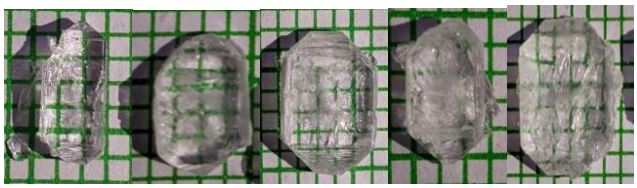

(1a) (1b) (1c) (1d) (1e)

Figure 1. Grown crystal of (a) Pure KDP, (b to e) (0.2, 0.4, 0.6 and 0.8) wt% LOMHC doped KDP

III. RESULTS AND DISCUSSION

A. *EDAX analysis*

EDAX analysis is used to determine the presence of dopant atoms in the produced crystals by using Philips XI-30. The data of EDAX analysis of pure and different wt% LOMHC doped KDP crystals are presented in the table 1.

Table 1. EDAX Result

Sample Number and Name	Carbon (C)	Potassium (K)	Oxygen (O)	Phosphorous (P)	Chlorine (Cl)
	Wt %				
1. Pure KDP	-	34.35	48.29	22.03	-
2. 0.2wt% LOMHC doped KDP	3.75	32.62	41.53	21.30	0.44
3. 0.4wt% LOMHC doped KDP	3.87	29.11	41.00	21.03	1.51
4. 0.6wt% LOMHC doped KDP	4.55	32.41	36.44	20.83	1.60
5. 0.8wt% LOMHC doped KDP	5.28	31.94	40.71	20.72	3.43

The chemical formula of potassium dihydrogen phosphate (KDP) is KH2PO4. Hence, the EDAX analysis of pure KDP shows the presence of potassium (K), phosphorous (P) and oxygen (O). The chemical formula of dopant l-ornithine monohydrochloride (LOMHC) is C5H13ClN2O2. Therefore, when it is doped into pure KDP, its EDAX analysis shows the presence of carbon (C) and chlorine (Cl), which indicates that dopant atoms are present in the KDP crystal. Further, moving towards specimen 2 to 5, as the wt% of LOMHC in KDP is increased, the wt% of carbon and chlorine are also observed to increase in LOMHC doped KDP crystal. This validates the doping operation's success.

B. *Powder XRD study*

Powder XRD patterns of pure KDP crystals (specimen 1) and other various weight% LOMHC doped KDP crystal (specimen 2-5) could be seen in Figure 2, while table 2 shows the unit cell parameters, cell volume, and X-ray density.

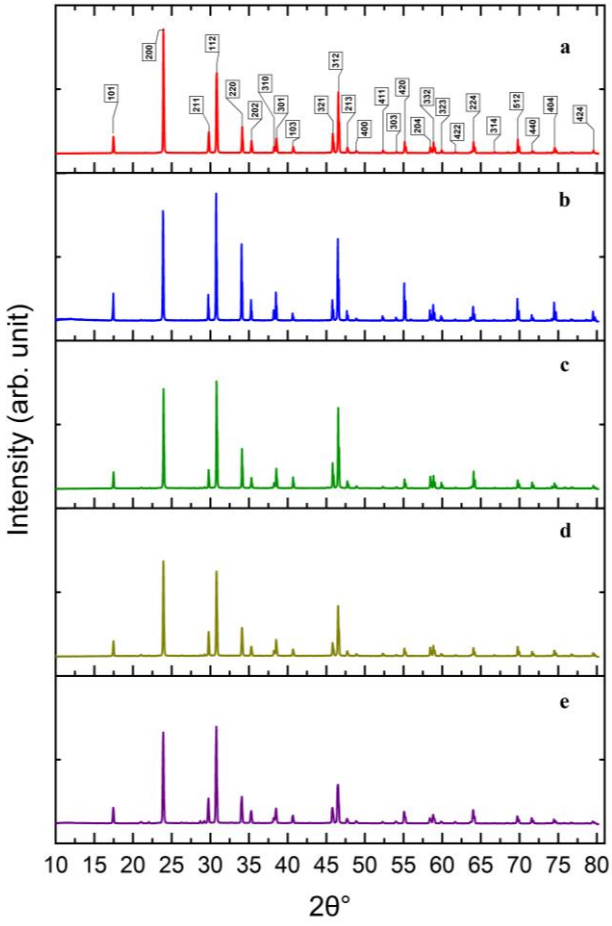

Figure 2. Powder XRD patterns of (a) specimen 1. Pure KDP (b) specimen 2. 0.2wt% (c) specimen 3. 0.4wt% (d) specimen 4. 0.6wt% and (e) specimen 5. 0.8wt% LOMHC doped KDP

Table 2. Unit cell parameters, cell volume and X-ray density of pure and LOMHC doped KDP crystals

Specimen Number	LOMH Doping (wt%)	a = b (Å)	c (Å)	Volume cell (Å^3)	X-ray density (g cm^{-3})
Specimen 1	0	7.4410	6.9646	385.62	2.3436
Specimen 2	0.2	7.4418	6.9788	386.49	2.3384
Specimen 3	0.4	7.4451	6.9639	386.00	2.3413
Specimen 4	0.6	7.4417	6.9697	385.97	2.3415
Specimen 5	0.8	7.4469	6.9742	386.76	2.3367

It is noticed that the primary diffraction pattern peaks of all these specimen at 2θ positions are around 17.455o, 23.929o, 29.777o, 30.807o, 34.104o, 38.53o, 45.837o, 46.558o, 55.146o, 58.887o, 64.03o and 69.757o which corresponds to the planes (101), (200), (211), (112), (220), (301), (321), (312), (420), (332), (224) and (512), respectively. These are in well agreement with the earlier results [9,10]. The crystal structure of LOMHC has been reported by Akio Chiba et al. [11]. It grows as a colourless plate from its aqueous solution and belongs to monoclinic crystal system having unit cell parameters: a = 10.21 Å, b = 8.04 Å, c = 4.98 Å; β = 97o; space group: P21 or P21/m. While KDP possesses tetragonal crystal system having space group I-42d. According to diffraction pattern in figure 2, It could be said that the presence of dopant

LOMHC does not indicate the presence of an additional phase in the various wt% LOMHC doped KDP crystals, implying that all of the crystals are single-phase with characteristic KDP peaks. The similar trend has been reported in the literature in terms of the effect of dopant in KDP [12]. The unit cell parameters of KDP crystal fits in nicely with standard JCPDS card no 35-0807 as well as with the report of other researchers [9,13,14]. KDP crystals, both pure and LOMHC doped, have a tetragonal space group I-42d tetragonal crystal system. Sharp xrd peaks imply that produced crystals are crystallinity-good. When LOMHC in different wt% is doped into pure KDP, a general observation indicates intensity decrement of the most prominent peak (200) of pure KDP observed at 23.929o and slight shift in position of this peak, shown in figure 3 with an expanded scale. The strains in the lattice may be responsible for this observation and slightly deformation in the crystal structure of doped KDP compared to pure KDP. The strain in the crystalline lattice is caused by a small degree of doping of the large size molecule LOMHC, which is reflected in a tiny change in the unit cell characteristics, X-ray density measurements as well as increase in volume of doped KDP crystals. Lattice characteristics rise as dopant concentration increases, potentially increasing the porosity of doped KDP crystals. Because the dopant LOMHC concentration is so low, the rate of taking in dopant particles may be slow compared to the rate of deposition of growth elements, resulting in a rise in the doped KDP crystals' lattice parameter values. The slight shift in the position of the peak of doped crystals suggests slightly distortion in the crystal structure of doped KDP compared to pure KDP [9,13].

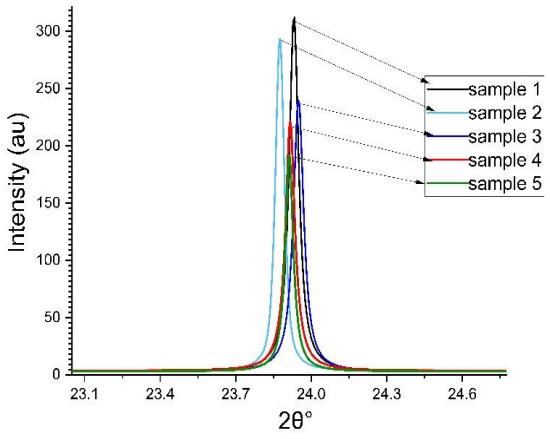

Figure 3. (2 0 0) diffraction peak of pure and LOMHC doped KDP crystals

Crystallite size and strain determination by using various methods

In the present study, the crystallite size and strain associated with the grown crystals due to doping of LOMHC in different wt% is determined by using various methods discussed below.

→ **Crystallite size determination from the Scherrer method**

The average crystallite size is determined by using highly intense crystalline plane (200) based on the Scherrer equation:

$$D = K\lambda/\beta D\cos\theta,$$

where D represents the crystallite size, K is taken 0.9 as the shape factor, λ represents wavelength of the X-ray source. In the present case, it is CuKα radiation having value of wavelength 1.5406 Å. βD and θ stand for the FWHM (broadening of the peak) in radian and the peak position in radian.

→ **Crystallite size and strain determination from the Williamson-Hall method**

The crystallite size and strain are determined by applying Williamson-Hall (W-H) method [15] to the powder XRD patterns. The equation can be expressed as:

$$\beta\cos\theta = \varepsilon WH\,(4\sin\theta) + K\lambda/DWH,$$

where, β represents the total broadening of the high-intensity diffraction peaks due to crystallite size and strain, DWH is the crystallite size, εWH is the strain, shape factor K as 0.9 and λ is the source wavelength 1.5406 Å. The crystallite size (DWH) and lattice strain (εWH) is calculated from the intercept and slope of the linear fit of the graph between 4sinθ on x axis and βcosθ on y axis.

→ **Crystallite size and strain determination from the Halder-Wagner method**

The technique proposed by Halder and Wagner is additionally been utilized to decide crystallite size along with strain. A model proposed by Halder and Wagner can be expressed by the equation [16]

$$\left(\frac{\beta}{\tan\theta}\right)^2 = \frac{K\lambda}{D_{HW}}\cdot\frac{\beta}{\tan\theta\sin\theta} + 16\,\varepsilon_{HW}^2$$

The linear fit data of the slope of the H-W plot of $\left(\frac{\beta}{\tan\theta}\right)^2$ on the y axis against $\frac{\beta}{\tan\theta\sin\theta}$ on the x axis yield the crystallite size (DHW) and the y intercept yield the value of lattice strain (εHW).

→ **Crystallite size and strain determination from the Wagner-Aqua method**

A method proposed by Wagner and Aqua is likewise and equation can be expressed as [17]

$$(\beta\cos\theta)^2 = (4\varepsilon_{WA}\sin\theta)^2 + \left(\frac{K\lambda}{D_{WA}}\right)^2$$

All the observed reflections in the 2θ range shown in the figure 2 are considered to draw W-A plot between (4sinθ)2 on the x axis and (βcosθ)2 on the y axis. The slope and intercept on vertical axis of the linear plot yield lattice strain value (εWA) and the crystallite size value (DWA).

→ **Stacking fault calculation**

The stacking fault (SF) values have been calculated by using the equation [18,19]

$$SF = \left[\frac{2\pi^2}{45(3\tan\theta)^{1/2}}\right]\beta$$

The values of stacking fault (SF), crystallite size along with strain evaluated by several methods are tabulated in table 3.

Table 3. Stacking fault (SF), crystallite size and strain values of pure and LOMHC doped KDP crystals measured from several methods.

Specimen No	SF × 10^{-4}	Scherrer Method D (nm)	W – H Method		H – W Method		W – A Method	
			D_{WH} (nm)	ε_{WH} × 10^{-4}	D_{HW} (nm)	ε_{HW} × 10^{-4}	D_{WA} (nm)	ε_{WA} × 10^{-4}
1	19.52	39.76	46.37	6.74	39.27	8.45	40.90	13.66
2	17.44	39.78	48.99	7.31	40.66	8.56	42.14	13.75
3	17.26	39.91	49.70	7.46	41.00	9.26	42.40	13.80
4	19.38	40.14	51.54	8.20	41.26	10.03	42.53	14.75
5	17.43	40.17	54.80	11.80	42.27	12.7	43.00	18.13

Table 3 shows that as the weight percent of dopant LOMHC increases, the value of crystallite size and strain increases. Also, noticeable that the calculation from Scherrer equation is nearly similar to the values calculated from H – W and W – A methods, while W – H method gives larger values than the values obtained from the Scherrer method and others. This is because only size broadening is considered in the Scherrer method, while in the W – H method, both size and strain broadening of diffraction peaks are considered. An increasing pattern of crystallite size as well as lattice strain is found in all analytical methods after increasing the wt% of dopant LOMHC from 0.2wt% to 0.8wt% moving from sample 1 to 5. An increase in crystallite size may suggest the facilitation in the development of crystallites. A smaller crystallite would result in a larger FWHM. [20]. In the present case, increase in crystallite size results into reduction in the FWHM. Further, an increase in stacking faults relates to the XRD peaks [20]. In the present case, stacking fault reduces as wt% of dopant increases in moving from sample 1 to 5, which again results into reduction in FWHM. An increasing value of strain results into decrease in the intensity of the peak. All the changes in the FWHM and peak intensity are clearly visible in the figure 3.

C. SHG Analysis

To verify NLO characteristic, Kurtz powder test using Q switched High Energy Nd:YAG Laser with modulated radiation of wavelength 1064 nm, having repetition rate 10 Hz and pulse width 6 ns on the powder of crystals through a visible blocking filter was done. To acquire the most powder SHG, the input laser beam was focused at the crystal powder. The emission of green light having wavelength of 532 nm indicated the creation of a second harmonic signal in crystals. This confirms the NLO behaviour. The NLO SHG efficiency is calculated using monocrystalline powder of KDP as reference material using the equation:

SHG Efficiency = Output Energy (sample)/Output Energy (KDP)

The SHG efficiency of pure and LOMHC doped KDP crystals are listed in the table 4.

Table 4. SHG efficiency of pure and LOMHC doped KDP crystals

Sample	Output Energy (mJ)	Input Energy (J)	SHG Efficiency
Pure KDP (Sample 1)	7.50	0.70	1
0.2wt% LOMHC doped KDP (Sample 2)	6.81	0.70	0.908
0.4wt% LOMHC doped KDP (Sample 3)	5.89	0.70	0.785
0.6wt% LOMHC doped KDP (Sample 4)	4.31	0.70	0.574
0.8wt% LOMHC doped KDP (Sample 5)	4.17	0.70	0.556

The SHG efficiency evaluated with regard to KDP decreases in the case of LOMHC doped KDP and increases when the wt% of dopant LOMHC is increased, as shown in table 4. The decreased SHG efficiency of doped KDP has been reported by several researchers [10,21]. Decrease in SHG efficiency of pure KDP after LOMHC doping indicates that side chain might not be acted as a proton donor. The proton may not be placed into the structure of KDP by LOMHC doping, resulting in a reduction in SHG efficiency of KDP. Further, the presence of dopant might have affected the non-centrosymmetric packing of the molecular crystal of KDP; resulted into reduction in the SHG efficiency of LOMHC doped KDP. In other words, depressed SHG efficiency of LOMHC doped KDP indicates an unfavourable molecular alignment for nonlinearity.

D. UV-Vis Analysis

The optical study was recorded by UV-1700 series spectrometer in the wavelength range of 190-800 nm. Figure 4 shows optical transmittance spectra of pure and LOMHC doped KDP crystals.

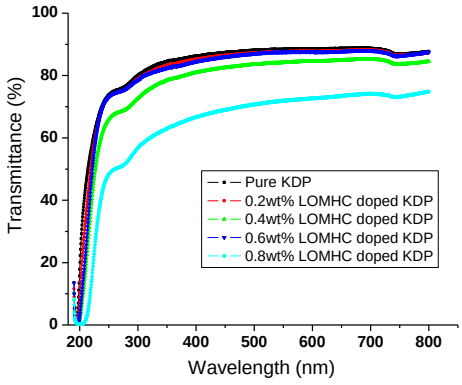

Figure 4. Transmission spectra of pure and LOMHC doped KDP

In the visible region, the spectra have a great degree of transparency. The transmittance value decreases very slightly after 0.2wt%, 0.4wt% and 0.6wt% doping of LOMHC but remarkable reduction is observed in the case of 0.8wt% doping of LOMHC into KDP. The cut off

wavelength of 195 nm is observed for pure and 0.2wt% LOMHC doped KDP, 200 nm for 0.4wt% and 0.6wt% and 213nm for 0.8wt% LOMHC doped KDP. The remarkable reduction in transparency and shifting of cut off wavelength towards higher wavelength side in the case of 0.8wt% LOMHC doped KDP indicates the optimum influence of a dopant on transmittance. For all the crystals, the transmittance% within optical region along with cut off wavelength is shown in the table 5.

Table 5. Transmittance and optical energy band gap (Eg) values of pure and LOMHC doped KDP crystals

Specimen	Transmittance% within visible range	Band gap energy (eV)	Cut off wavelength (nm)
Pure KDP Specimen 1	85.59% to 88.72%	6.19	195
0.2 wt% LOMHC doped KDP Specimen 2	84.46% to 88.12%	6.13	195
0.4 wt% LOMHC doped KDP Specimen 3	83.58% to 87.98%	6.06	200
0.6 wt% LOMHC doped KDP Specimen 4	80% to 85.27%	6.00	200
0.8 wt% LOMHC doped KDP Specimen 5	65.43% to 74.17%	5.67	212

Determination of optical energy band gap

The Tauc relation was used to calculate the optical energy band gap (Eg) for pure and LOMHC doped KDP crystals. [22]:

$$\alpha h\nu = A(h\nu - Eg)n,$$

Where, h is Planck constant, ν represents frequency of incident photon, A is constant, Eg is the average band gap of the material and n stands for index that is affected by different kinds of transitions. The value of the index n = 1/2, 3, 2 and 3/2 denotes allowed direct transition, forbidden indirect transition, indirect allowed transition and forbidden direct transition, respectively [23]. α is the optical absorption coefficient and is calculated by using the standard formula [24]:

Tauc's plot is shown in the figure 5 for pure and LOMHC doped KDP crystals.

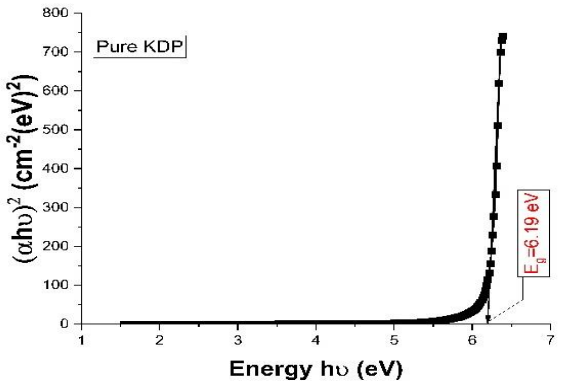

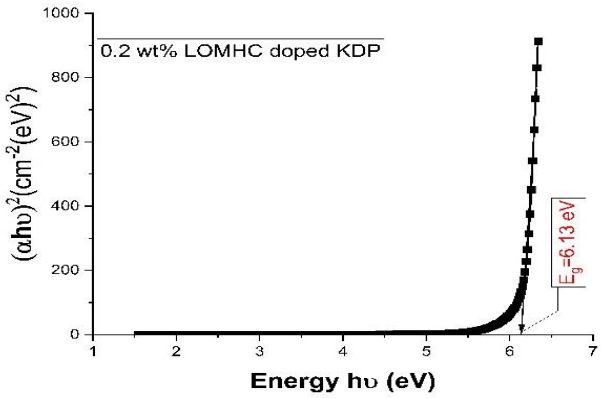

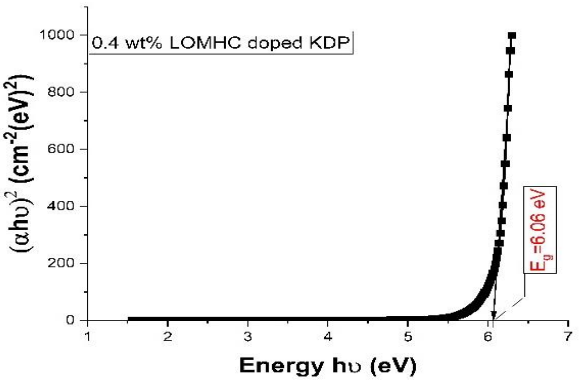

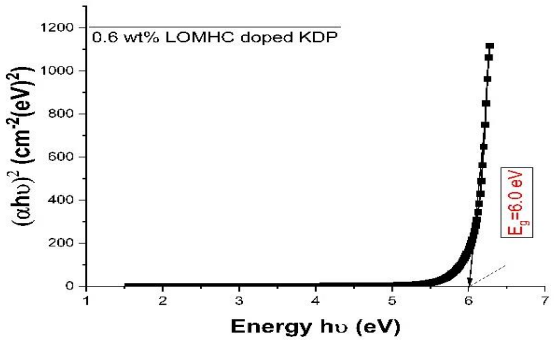

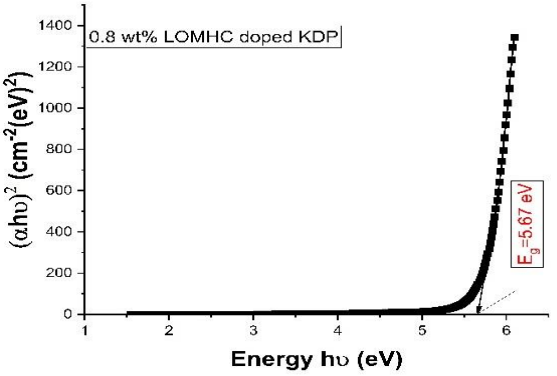

Figure 5. Tauc's plot of pure and LOMHC doped KDP crystal

In the figure 5, the graphs are plotted between (αhν)2 vs energy (hν). By projecting the tangent of the linear part of the graph to the X-axis gives the optical energy band gap (Eg) value.

The results mentioned in table 5 indicate that the LOMHC doped KDP shows gradual reduction in the value of energy band gap. Though, the fairly good value of energy band gap of pure and LOMHC doped KDP indicates that the generated crystals are acceptable for optoelectronic device manufacture [25]. The ability of a dielectric medium, such as a crystal, to be polarized under the influence of applied radiation is demonstrated by the energy band gap of the crystal. [24]. For a crystal, having high value of energy band gap indicates its better ability to be polarized. The reduction in Eg of LOMHC doped KDP can be attributed the formation of recombination centre, the energy level of which is situated in the forbidden band that able to recombine with the conduction electrons and holes [26].

E. Complex impedance and modulus analysis

The complex impedance and modulus of pure and LOMHC doped KDP crystals were analysed at room temperature in the frequency range of 100 Hz to 1 MHz in current study. The data obtained by the LCR meter was utilised to analyse dielectric constant (ε'), dielectric loss (ε'), ac and dc conductivity (σac and σdc) and real (Z') and imaginary (Z'') parts of complex impedance (Z*). The formulas given in the literature [27] have been used for the same.

Frequency dependence of real component of impedance

Figure 6 show the reliance of real component of complex impedance (Z') on frequency at room temperature of pure and LOMHC doped KDP.

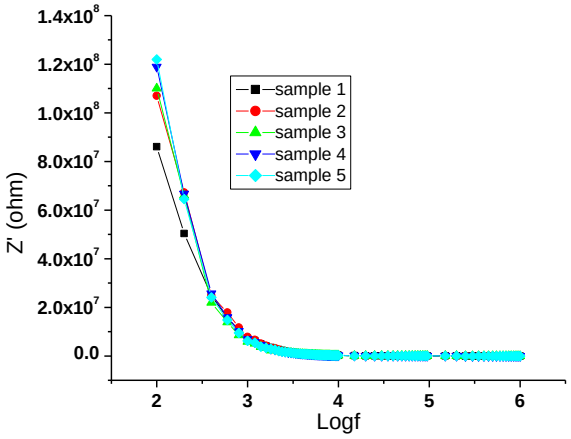

Figure 6. Plot of Z' versus logf of sample 1 pure KDP and samples 2 to 5 (0.2, 0.4, 0.6 and 0.8) wt% LOMHC doped KDP

Figure 6 implies that Z' decreases with increase in frequency trend along with all five specimens, indicating conductivity inversely proportional to frequency and the presence of space charge conduction at low frequencies. At high frequencies, for all the samples, Z' becomes frequency-independent, suggesting that space charge is unable to follow a high frequency field. For low-frequencies, for a specific value of 100 Hz, the value of Z' increases as the concentration of dopant increases from 0.2wt% to 0.8wt%. This indicates that when the doping concentration grows, the value of dc conductivity decreases. As dopant LOMHC is added to pure KDP, a frequency at which Z' becomes frequency independent is found to shift to the lower frequency side. This suggests that the samples have a frequency relaxation operation, which leads in a shorter grain and/or grain boundary relaxation time. In the following part, the same is evaluated and tabulated. Thus, in terms of conductivity and grain and/or grain boundary relaxation time of pure KDP, the effect of dopant and its concentration is easily visible.

Frequency dependence of real component of modulus

Figure 7 represents the real component of complex modules (M') dependency on frequency at room temperature of pure and LOMHC doped KDP.

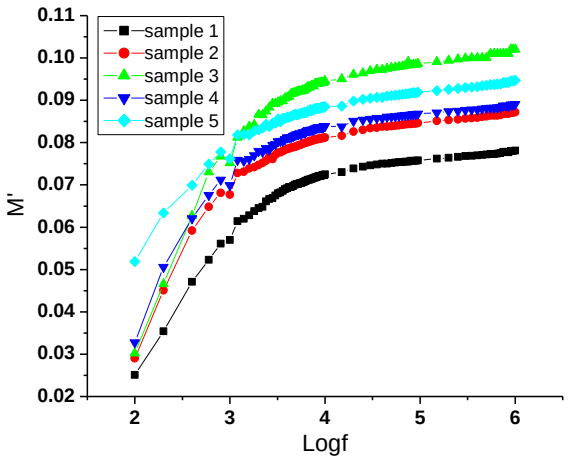

Figure 7. Plot of M' versus logf of sample 1 pure KDP and samples 2 to 5 (0.2, 0.4, 0.6 and 0.8) wt% LOMHC doped KDP

The M' values for all of the samples are small, as can be seen in Figure 7. This signifies that the electrode polarization has been removed. [28-30]. With an increase in frequency, M' values of all the samples increase and attain maximum and almost saturate value in the high-frequency region. This can be attribute to the distribution of relaxation processes over a range of frequencies and the presence of space charge polarization [30-32]. As the frequency increases, the dispersion in the values of M' of all the samples is observed which can be attribute to the conductivity relaxation, indicating the presence of relaxation time, accompanied by loss peak in the low frequency region in the plot of imaginary part of electric modulus (M'') versus log of frequency. As LOMHC is doped into KDP and as its weight% increases from 0.2wt% to 0.8wt%, M' value increases in the lower as well as higher frequency region. Raise in the M' values with dopant concentration, indicates decrease in the mobility of the charge carriers, which ultimately results into decrease in the value of dc although ac conductivity of the samples. This is discussed in the conductivity analysis section. Further, M' value for all the samples show continuous increase as frequency rise, that confirms the controlling of the conduction process because of the presence of short-range

mobile charge carrier [32,33]. It is also observed from the figure that for all the samples, the increasing rate of M' is more in the low frequency region compared to high frequency region, which indicates that at lower frequency the conduction event is controlled by the long-range mobility of the charge carriers [32,34].

Frequency dependence of imaginary component of impedance

Figure 8 show imaginary component of complex impedance (Z '') on frequency at room temperature of pure and LOMHC doped KDP is dependent.

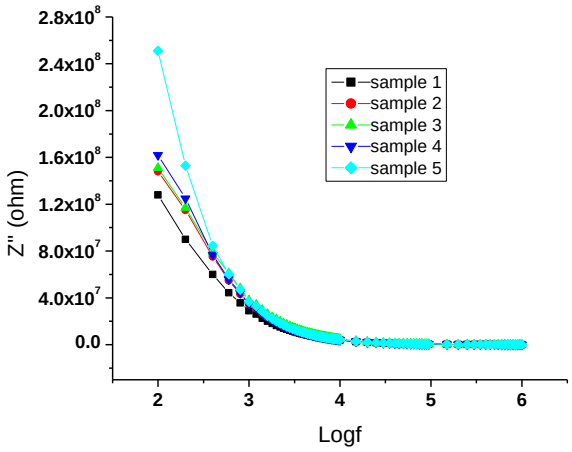

Figure 8. Plot of Z'' versus logf of sample 1 pure KDP and samples 2 to 5 (0.2, 0.4, 0.6 and 0.8) wt% LOMHC doped KDP

From the figure 8, it is observed that Z'' shows behavior similar to Z'. Generally, Z'' plot shows relaxation peak within low or high frequency region. In the present case, the relaxation peak is not observed in any of the sample within the frequency range under study, which may be due to weak current dissipation in the materials as decrease in the mobility of the charge carriers with increasing dopant concentration or beyond the limit of lower frequency measurement. As LOMHC is doped into KDP and as its weight% increases from 0.2wt% to 0.8wt%, the height of Z'' plot increases. The height of Z'' plot is proportional to grain and/or grain-boundary resistance, whatever is dominant in the sample. This can be expressed by the equation:

$$Z'' = R\omega m\tau/1+\omega m2\tau2,$$

Where, ωm is the relaxation angular frequency which can be found from the relaxation peak in the Z'' plot. Hereby, as the relaxation peak is not observed in the Z'' plot, the same can be found by fitting the impedance plane plot by using the software Z-view. R is the grain and/or grain-boundary resistance, whatever is present and/or dominant in the sample and τ prefers the relaxation time. The increased height of the Z'' plot with increase in dopant concentration clearly indicates the increase in the value of grain and/or grain-boundary resistance, which are discussed in the complex impedance plane plot analysis. From the figure 6, Also the imaginary part of the impedance (Z'') for all the samples becomes independent of frequency at high frequencies, which may be due to release of space charge in the material [35-38].

Frequency dependence of imaginary component of modulus

Figure 9 shows the relationship of the imaginary component of complex modulus (M '') on frequency at room temperature of pure and LOMHC doped KDP.

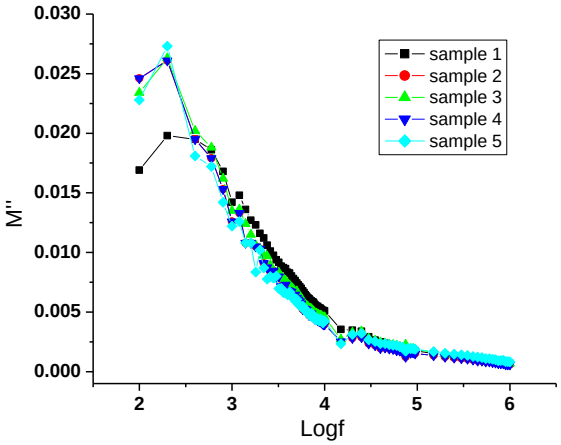

Figure 9. Plot of M'' versus logf of sample 1 pure KDP and samples 2 to 5 (0.2, 0.4, 0.6 and 0.8) wt% LOMHC doped KDP

From the figure 9, it is observed that within the frequency range under study, i.e., 100 Hz to 1MHz, M'' values are large for all the samples in the low frequency range compared to high frequency range. The large values of M'' for each at lower frequency range can be attribute to the small value of capacitance due to electrode polarization effect resulting small amount of charge carriers at the electrode electrolyte interface. In low frequency range, M'' curves of pure as well as LOMHC doped KDP samples exhibit peak at the same frequency, i.e., at 200 Hz, with increase in peak height in this doped crystal. Compare to pure KDP, increase in M'' in the case of LOMHC doped crystals can be attribute to decrease in ionic conductivity as well as the dependence of capacitance of grain and/or grain boundary on the dopant. The appearance of peak at the same frequency, i.e., 200 Hz after LOMHC doped into KDP indicates the conductivity of charge carriers may not be dopant activated. Moving to lower frequency from higher, the existence of a peak in all samples shows a change in charge carrier mobility from short to long range. The dopant-dependent hopping process of electrical charge transfer can be used to explain this phenomenon. The appearance of the peak at the same frequency after LOMHC doped into KDP, indicates that the transition point of the mobility of the charge carriers from short to long range does not depend on the dopant LOMHC or its concentration in KDP and hence the leakage current in the samples due to hopping phenomenon may not be dopant activated or it may be independent of dopant LOMHC and its concentration in pure KDP.

Complex modulus spectrum

Figure 10 shows the complex modulus spectrum at room temperature for pure and LOMHC doped KDP.

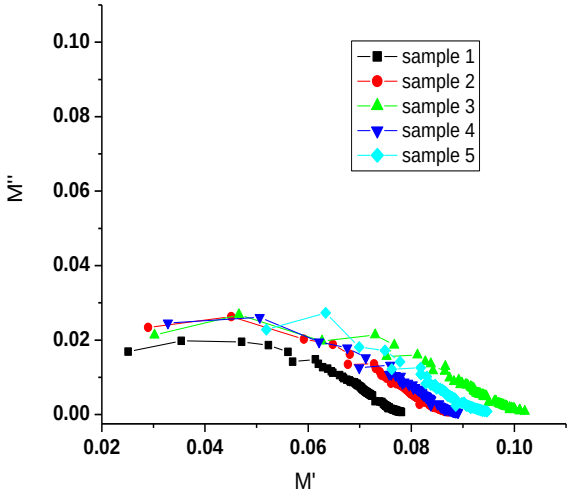

Figure 10. Complex plane plot of M'' versus M' of sample 1 pure KDP and samples 2 to 5 (0.2, 0.4, 0.6 and 0.8) wt% LOMHC doped KDP

In the complex plane plot of electric modulus shown in figure 10, the prominent arc is observed for pure KDP as well as LOMHC doped KDP crystals of samples 1 to 5. The low capacitance of bulk, i.e. grain, is responsible for this arc, suggesting the presence of grain contribution mainly. For all the formed crystals of samples 1 to 5, the segments of the grain arc from the intersection on the M' axis are obviously visible. From the plot of figure 10, clearly visible that compared to pure KDP crystal, the arcs show increased diameter for LOMHC doped KDP, indicating decrease in the value of grain capacitance. The curves of the formed crystals have the shape of depressed semicircles with their centers below the real axis, indicating that they do not meet the criteria for an ideal Debye model. This shows a deviation from ideal behaviour, indicating relaxation behaviour of the non-Debye kind. The semicircles demonstrate relaxation widening, indicating that the electrical relaxation in the formed crystals is not of the Debye type.

Scaling behaviour of M''

The study of scaling tendency of Z" and M" is highly important in order to acquire more knowledge about the influence of the relaxation dynamics on several variables like as temperature, structure, and charge carrier concentration [30,39]. In the present case, the scaling behaviour of M'' at room temperature for pure KDP and LOMHC doped KDP is carried out. The scaled imaginary part of electric modulus is shown in the figure 11. The Mmax'' and fmax are used as the scaling parameters for M'' and f, respectively.

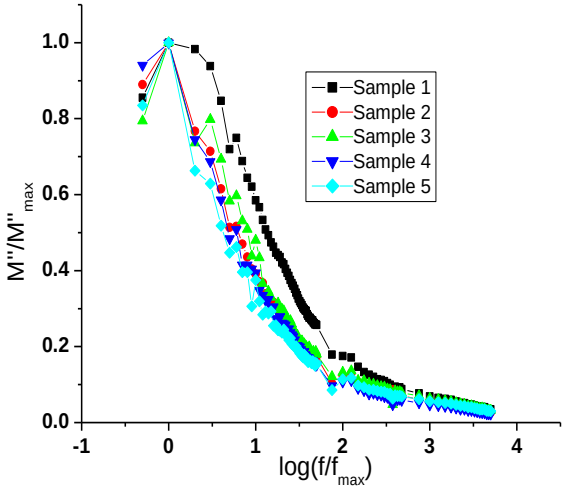

Figure 11. The scaling of M'' of sample 1 pure KDP and samples 2 to 5 (0.2, 0.4, 0.6 and 0.8) wt% LOMHC doped KDP

It can be seen from the figures 11 that the modulus spectra of samples 1–5 overlap but do not blend into a single master curve, indicating that they are still distinct enough to be identified, particularly, pure KDP and LOMHC doped KDP are clearly identified. As the current process is carried out at room temperature to examine the effect of doping of LOMHC on impedance and modulus properties of crystals of pure KDP, the result indicates that the charge carrier concentration affects the relaxation dynamics, which may vary as per the wt% of the dopant LOMHC. The asymmetrical shapes of the plots indicate the deviation of dielectric relaxation process from the pure Debye behavior and existence of distribution of relaxation times. The non-symmetric normalized modulus plot of figure 11 is in keeping with the electrical function's non-exponential nature, which may be effectively represented by the Kohlrausch-William-Watts exponential function [30,39,40] as per the equation:

$$\phi = \exp\left[\left(-\frac{t}{\tau}\right)^{\beta}\right]$$

Where, β is an exponent having values lies within 0-1, implying deviation from the Debye relaxation. The value of β can be calculated as per the equation [30,41]

$$\beta = \frac{1.14}{FWHM}$$

Here, FWHM is the full width at half maximum of M'' versus logf curve and obtained from Gaussian type curve fitting.

The calculated values of exponential parameter β for grain relaxation are shown in the table 6.

Table 6: Exponent parameter (β) values for all the samples 1 to 5

Sample Name	β value
Pure KDP	0.65
0.2wt% LOMHC doped KDP	0.62
0.4wt% LOMHC doped KDP	0.55
0.6wt% LOMHC doped KDP	0.54
0.8wt% LOMHC doped KDP	0.52

The highest value of the exponent variable β, i.e., β = 1, denotes Debye type relaxation, whereas the lower the value of, the greater the variation of relaxation from Debye type relaxation. In the present case, smaller value of β indicates non-Debye type relaxation is presented within pure as well as LOMHC doped KDP crystals.

Complex impedance spectrum

The complex impedance spectrum is studied to gain a better understanding of the polarization processes that occur in formed crystals at ambient temperature. Because each of these resistances has a distinct relaxation period, resulting in discrete semicircles in the complex impedance plane plot, this figure helps to separate out the resistances associated to grain, grain boundaries, and film/electrode interfaces.

Figure 12 illustrates the complex impedance plane plot at ambient temperature of pure KDP and various wt% LOMHC doped KDP.

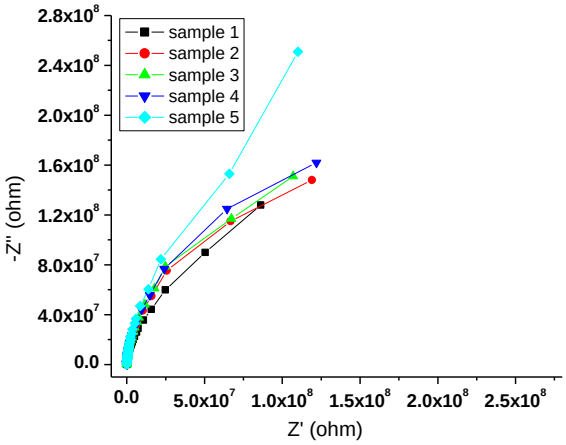

Figure 12. The complex impedance plane plot of Z'' versus Z' of sample 1 pure KDP and samples 2 to 5 (0.2, 0.4, 0.6 and 0.8) wt% LOMHC doped KDP

The curves show bending towards real axis-Z'. The exploration of full, partial, or no semicircles is determined by the intensity of relaxation and the frequency range available [42,43]. For each sample, the high frequency arcs pass through the origin. The centre of each semicircle arc stays below the real axis, resulting in depressed semicircles, confirming the presence of a non-Debye type of relaxation in all samples. The impedance property of the material under study is defined by the existence of single, double, or more semi-circular arcs, the pattern of which changes as the sample temperature or the wt % or mol % of the additives changes. Total impedance of the polycrystalline material has contribution of grain, grain boundaries and sample/electrode interface [44]. In the present case, the absence of any second arc in pure as well as in LOMHC doped KDP, confirms that the polarization mechanism in all the samples corresponds to bulk effect arising in the grains. Further, the absence of any residual semicircle at low frequencies in all the samples indicates the absence of contact or electrode effect, probably due to the well-polished surface of the samples and electrode. The effect of dopant LOMHC and its concentration on impedance characteristics of pure KDP is clearly visible in the form of gradually changes of the appearance of semi-circular arcs of LOMHC doped KDP samples 2 to 5. Assume equivalent circuit of these tendency, it evaluates understanding of relation between microstructure and ongoing electrical phenomenon. In current case, fitting of complex impedance plot of each one shows each holds only grain effect behavioural certain region against entire frequency range. In general, the impedance pattern's semi-circular arcs may be referred to a parallel pair of resistance and capacitance as in figure 13.

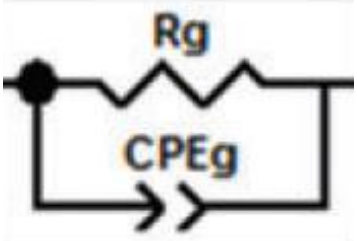

Figure 13. Equivalent R-CPE circuit

Due to non-ideal capacitive behaviour, the CPE, meaning Constant Phase Element, is used in the circuit instead of capacitance. The capacitance values for each specimen are evaluated using the equation presented in the literature [45]. Hence, major role of grain effect only, R is representing grain resistance that could be gained from intercepting every semicircle with real axis. Also, figure 12 gives visuals of gradually increasing diameter of semicircle tendency as going from pure-undoped KDP to 0.8 wt% LOMHC doped, i.e., samples 1 to 5. These suggest an increase in grain resistance and, consequently, a reduction in conductivity. The values of the grain resistance and capacitance are collected in Table 7.

Table 7. Equivalent circuit parameters for the samples 1 to 5

Sample-label	R_g (MΩ)	C_g (pF)	τ_g (ms)	α_g
Pure KDP	135	4.83	0.652	0.9744
0.2wt% LOMHC doped KDP	205	4.25	0.871	0.9783
0.4wt% LOMHC doped KDP	237	3.74	0.886	0.9770
0.6wt% LOMHC doped KDP	226	4.22	0.953	0.9806
0.8wt% LOMHC doped KDP	281	4.08	1.146	0.9807

The relaxation time for grain was evaluated by relation $\tau g = Rg \cdot Cg$. Here, αg represents the degree of deviation for grain. Table 7 shows that the grain relaxation time is longer in LOMHC doped KDP. This suggests that the presence of dopant LOMHC reduces the relaxing process of the grain present. Moreover, αg raises to value one for LOMHC doped KDP crystals of samples 2 to 5, implying the system tends to the ideal capacitive behaviour.

F. Dielectric analysis

Frequency dependence of real part of dielectric constant

The frequency dependence of real part of dielectric constant, i.e., ε' of pure and different wt% LOMHC doped KDP crystals are shown in the figure 14.

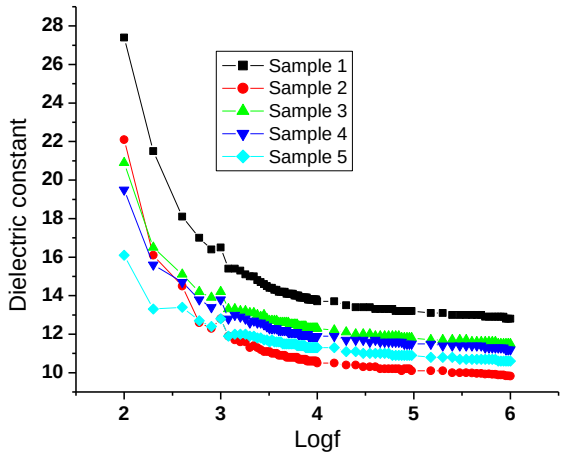

Figure 14. Plot of dielectric constant versus logf of sample 1 pure KDP and samples 2 to 5 (0.2, 0.4, 0.6 and 0.8) wt% LOMHC doped KDP

Pure as well as LOMHC doped KDP crystals show high value of dielectric constant in lower frequency region, which can be considered as a normal dielectric behaviour [46]. Then as the frequency of the applied field is increased, the dielectric constant value of all the samples begins to decrease. This is related to the dipoles' failure to follow the field fluctuation at high frequencies, as well as the polarization effect. At high frequencies, the frequent reversal of the electric field is so quick, which results into no excess ion diffusion in the direction of the applied field. The overall response of the dielectric constant of the material is cause of electronic, ionic, dipole and space charge polarization corresponding to frequencies 1015, 1013, 1010 and 102 Hz, respectively [47]. Below 100 Hz frequency, all the four polarization mechanisms contribute in the effective value of dielectric constant, while above 100 Hz there is no contribution of space charge polarization to dielectric constant value [32]. In the present case, the decrease in the dielectric constant value is significant within 100 Hz to 1 kHz which can be associated with the mobile ion and dipole polarization and then there is no significant change is observed. It is also observed that low frequency dispersion is highest in pure KDP rather than LOMHC doped KDP. It suggests that doping LOMHC into pure KDP lessens interfacial polarization and mobile ions. The interfacial polarization is not significant at high frequencies, hence dielectric constant remains relatively constant [48,49]. Further, the dielectric constant value is observed to decrease within the whole frequency range under investigation when LOMHC is doped into pure KDP. This indicates that the presence of dopant impedes the diffusion of ions in the space charge polarization and orientation of the molecules in the direction of the field. Microelectronics industry needs materials as an interlayer dielectric having low dielectric constant [50]. In the present case, doping of LOMHC reduces the dielectric constant of pure KDP from nearly 28 to 16; hence, such material may be useful to microelectronics industry.

Frequency dependence of imaginary part of dielectric constant

The frequency dependence of imaginary part of dielectric constant (ε''), i.e., dielectric loss of undoped and different wt% LOMHC doped KDP crystals are shown in the figure 15.

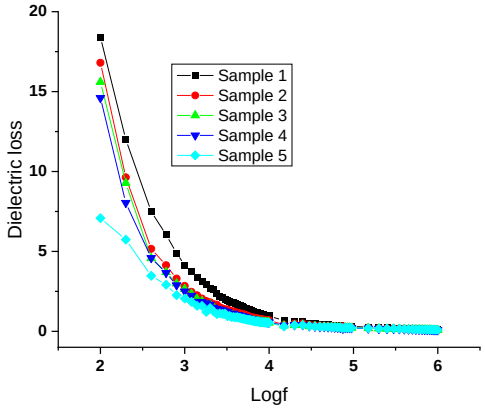

Figure 15. Plot of dielectric loss versus logf of sample 1 pure KDP and samples 2 to 5 (0.2, 0.4, 0.6 and 0.8) wt% LOMHC doped KDP

For LOMHC doped-undoped KDP, the nature of the plots is same, i.e., the higher values within lower frequency range and starts decreasing as frequency increasing. For all the samples, the comparison of dielectric loss curves (figure 15) with the dielectric constant curves (figure 14) shows that the dispersion in dielectric loss is more than that in dielectric constant, which indicates the impact of dc conductivity. The value of low frequency slope of dielectric loss versus log of frequency plot for all the samples is nearly -1, which indicates the dominancy of the dc conduction in this frequency region [51]. Now, the contribution to the dielectric loss generally consists of three different types, namely, relaxation loss, conduction loss and resonance loss. The relaxation loss is generated due to the relaxation polarization when the polarization process cannot comply with the speed of change of direction of external field. Hence, relaxation loss is observed in this high-frequency range. The resonance loss is observed when the frequency of external electric field is very high, i.e., of the order of 1013 Hz or more. In this frequency region, the vibration of electrons, atoms and molecules releases heat and results in resonance absorption [32,52,53]. As the upper limit of frequency in the present study is 106 Hz, the resonance loss is not observed. The conduction loss is caused by the sample's conductivity since the prepared samples may not act as an ideal insulator. A relation between dielectric loss and conductivity is given by the equation:

$$\sigma = \omega\varepsilon_0\varepsilon'',$$

Where, ω is the angular frequency of the applied electric field, ε0 is the vacuum dielectric constant and ε'' is the dielectric loss. The loss curve of all the samples shows highly dispersive nature in the low frequency region and dc conduction is dominant. So, this equation can be written as:

$$\sigma dc = \omega\varepsilon_0\varepsilon''.$$

As a result, the increased amount of dielectric loss in the low frequency zone may be attributed to the impact of dc conduction. As LOMHC is doped into pure KDP and as its weight% increases from 0.2wt% to 0.8wt%, the loss value gradually decreases, which indicates the gradual reduction in the dc conductivity value of the LOMHC doped KDP samples. The dc conductivity values of all the samples are found out and listed in the table given in the next section of ac conductivity analysis.

G. AC conductivity analysis

The ac conductivity (σac) values were evaluated by using the formula σac = ωεoε'', here ω is the angular frequency, εo is the permittivity of free space and ε'' is the dielectric loss [54].

Figure 16 shows the ac conductivity variation with respect to frequency for all the samples.

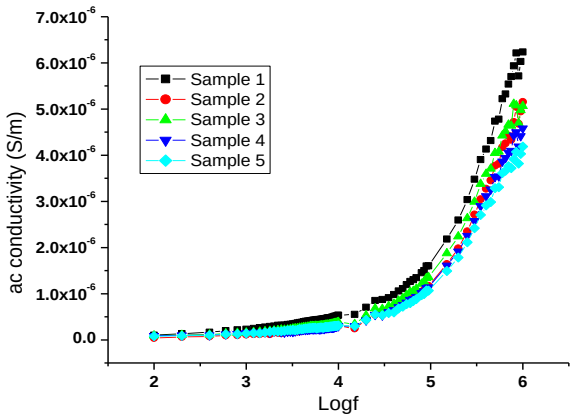

Figure 16. Plot of ac conductivity against logf of sample 1 pure KDP and samples 2 to 5 (0.2, 0.4, 0.6 and 0.8) wt% LOMHC doped KDP

On observing figure 16 implies that within the measured frequency range, the frequency dependent conductivity of pure and LOMHC doped KDP shows two different regions (i) a low frequency plateau region and (ii) a high frequency dispersion region. In the first one (i), up to a specific frequency value, the conductivity of all samples stays frequency independent. and hence can be characterized to the prepared samples' dc conductivity. The value of dc conductivity for all the samples can be estimated from extrapolating each line of the plot up to Y-axis [27]. Ions can move more quicker and shift from one spot to another within this frequency range. The successful ion jump to a nearby unoccupied site leads to the dc conductivity [55]. After a low frequency plateau zone, there occurs a high frequency dispersing region. The cross-over frequency from the region of frequency independent conductivity to the region of conductivity dispersion is known as hopping frequency (ωp) and this frequency cross-over shows that the conductivity relaxation phenomenon is occurring in the samples. The following empirical formula can be used to represent the frequency dependence of ac conductivity. [56-58]:

$$\sigma(\omega) = A\omega s,$$

where, ω = 2πf represents angular frequency of the ac signal, A is a constant defining polarizability strength of the material [59], s is an exponent indicating the amount of interaction either between mobile ions and lattice or charge carriers involved in the polarization process, the magnitude of which lies between zero and one [59,60]. The exponent s has been observed to behave [61-63] in different forms like a constant, either decreasing or increasing with temperature [60]. It means, exponent s depends on frequency and temperature [27]. Funke [62] has given the physical significance or physical meaning of the value of s. According to him, $s \leq 1$ and $s > 1$, would indicate the hopping motion involved is a (i) translational motion with a sudden hopping and (ii) localized hopping of the species with a small hopping without leaving the neighbourhood [64]. The value of exponent s one, i.e., s = 1 can be attribute to Debye case, generally attainable [65] at very low temperatures and would indicate the least interaction between the charge carriers leading to the confirmation of the assumption that ac conductivity is predominant due to the relaxation dipole moment [27]. The decrease in the value of exponent s either due to change in temperature or as existence of dopant in the pure crystal would indicate increased interaction between the same [60] and s = 0 would indicate frequency independent or dc conduction [66].

By using log scale, the frequency impact of ac conductivity can be given by:

$$\log\sigma(\omega) = \log A + s\log\omega.$$

A plot between logσ(ω) on Y-axis and logω on X-axis is known as Jonscher's plot, which is shown in the figure 17. The values of s and A, respectively, can be obtained from the slope and intercept of the linear fit of Jonscher's plot.

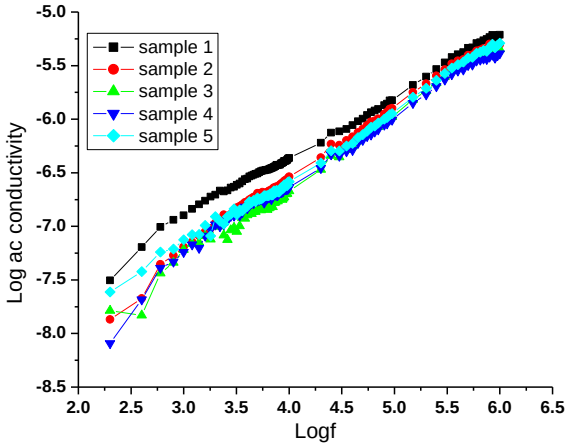

Figure 17. Jonscher's Plot of sample 1 pure KDP and samples 2 to 5 (0.2, 0.4, 0.6 and 0.8) wt% LOMHC doped KDP

The various conductivity mechanism relevant parameters of pure and LOMHC doped KDP crystals are listed in the table 8[67].

Table 8: Conductivity mechanism relevant parameters of pure and (0.2, 0.4, 0.6 and 0.8) wt% LOMHC doped KDP

Sample name	**$\sigma_{dc} \times 10^{-7}$ (S/m)**	**$\sigma_{ac} \times 10^{-6}$ (S/m)**	**s**	**$A \times 10^{-9}$ ($Sm^{-1}rad^{-n}$)**	**$Wm \times 10^{-2}$ (eV)**
Pure KDP	1.025	6.23	0.573	2.26	36.35
0.2wt% LOMHC doped KDP	0.935	5.15	0.658	0.66	45.39
0.4wt% LOMHC doped KDP	0.868	5.06	0.672	0.45	47.33
0.6wt% LOMHC doped KDP	0.812	4.58	0.64	0.65	43.12
0.8wt% LOMHC doped KDP	0.393	4.18	0.63	0.77	41.95

From the table 8, exponent-value lies between 0.5 and 1 for all the samples. Usually, in case of ionic conductors, 0.5-1 range can be attribute to the ideal long-range pathways and diffusion limited hopping [68]. Hence, doped-undoped KDP crystals possess the previously mentioned hopping mechanism. Further, the lowest value of s is obtained for the pure KDP crystal, that can be attribute to the high rate of successful jump of charge carriers, resulting into high value of dc conductivity [69], as shown in the table 8. As LOMHC is doped, the s-value rises. The same can be attribute to the reduced rate of successful jump of charge carriers, decreasing dc conductivity of LOMHC doped KDP, as shown in the table 8.

One can also notice from table 8, that polarizability strength A is highest in case of pure KDP but tends to decrease on doping. As direct relation in-between dielectric constant and polarizability of molecule implies that the stronger the polarizability of a molecule, the higher the material's dielectric constant[70]. Thus, the value of strength of polarizability of pure KDP and different wt% LOMHC doped KDP are in accordance with the dielectric results.
Table 8 also states that the ac conductive property at 1 MHz is highest for pure KDP rather than a doped one. This can be understood on the basis of a relation between exponent (s) and binding energy (Wm) as follows [71]:

$$1 - s = 6kBT/Wm,$$

Where, kB means Boltzmann constant, T represents absolute temperature, s is exponent and Wm indicates the binding energy. According to table 8, the binding energy is minimum for pure but increases on LOMHC doping. Rise in binding energy indicates the decreased amount of charge carriers crossing over the barrier. So that a decreasing tendency in the ac conductivity of LOMHC doped KDP crystals occurs. In addition, proton mobility within the environment of hydrogen bonds can be used to determine conduction in KDP group crystals [72]. It has been reported [12,72] that thermally generated L-defects and foreign particles incorporated into the lattice and forming L-defects determine the conductivity of KDP crystals. Like ammonium dihydrogen phosphate (ADP) [73], as protonic conduction in KDP is primarily owing to the anion (H2PO4)– instead of the cation (K+), the existence of more hydrogen bonds may diminish the L-defects, obstructing protons' movement. This could explain why doped samples have lesser ac conductivity than pure KDP samples.

IV. CONCLUSION

Slow solvent evaporation is utilized to grow pure and different weight% LOMHC doped KDP crystals at room temperature. The EDAX analysis confirms the successful doping of LOMHC. The powder XRD analysis confirms the single-phase behavior of each doped-undoped KDP crystals. The lattice strain and crystallite size of doped KDP crystals, calculated by various methods, are observed to increase. SHG analysis confirms the NLO behavior of all the crystals with reduction in efficiency of doped KDP crystals. UV-Vis analysis shows higher transparency among visible region with reduction in transparency and energy band gap value of doped KDP crystals. Complex impedance and modulus analysis confirm the existence of polarization mechanism in all the samples due to bulk effect arising in the grains. The related equivalent circuit parameters are calculated. The scaling behavior of modulus conforms the occurrence of relaxation dynamics within the samples are dependent on the concentration of the dopant LOMHC. The value of exponential parameter suggests non-Debye type relaxation within each specimen. The dielectric analysis shows normal dielectric behavior of all the samples. The doping of LOMHC reduces dielectric constant and loss values, making the material useful to microelectronics industry. An examination of ac conductivity reveals that all the samples follow the power law of Jonscher and the value of exponent s indicates the ideal long-range pathways and diffusion limited hopping mechanism in the samples.

ACKNOWLEDGMENT

The authors are thankful to Prof. H. P. Joshi (HOD, Physics) for his interest and author (Harshal Bhuva) is highly thankful to Prof. H. H. Joshi Sir and research scholar Miss. Laxmi Hathiya for his help in dielectric data collection.

REFERENCES

[1] X. Sun, X. Xu, Z. Gao, Y. Fu, S. Wang, H. Zeng, Y. Li, "Effect of EDTA on the Light Scatter in KDP Crystals," *J. Cryst. Growth*, **Vol.217, pp.404-409, 2000.**

[2] N. Zaitseva, L. Carman, I. Smolsky, "Habit Control during Rapid Growth of KDP and DKDP Crystals," *J. Cryst. Growth*, **Vol.241(3), pp. 363- 373, 2002.**

[3] K. D. Parikh, D. J. Dave, M. J. Joshi, "Crystal growth, thermal, optical, and dielectric properties of l-lysine doped kdp crystals," *Mod. Phys. Lett. B*, **Vol.23, pp.1589-1602, 2009.**

[4] N. Kanagathara, G. Anbalagan, "Growth, Optical and Dielectric Studies on Pure and L-Lysine Doped KDP Crystals," *International Journal of Optics*, **Vol.2012, pp.826763(1-6), 2012.**

[5] Sandhya Ravi, S. Chenthamarai, R. Jayavel, "FTIR, Electrical and SHG Studies of Single Crystals of KDP Doped with Phenylalanine," *IOSR Journal of Applied Physics*, **Vol.7(2), pp.39-44, 2015.**

[6] K. Rajesh, A. Mani, P. Praveen Kumar, "Growth, optical, Mechanical and Dielectric Properties of Promising NLO L-

Serine Potassium Di hydrogen Phosphate Single Crystals," *Int. J. Eng. Sci. Invention*, **Vol.1, pp.32-38, 2017.**

[7] O. V. Mary Sheeja, C. K. "Mahadevan, Growth and characterization of cds doped kdp single crystals," *International Journal of Research in Engineering and Technology*, **Vol.2(12), pp.738-748, 2013.**

[8] K. Mayilvani, R. S. Sreenivasan, "Spectroscopic characterization of pure and metal doped KDP single crystals," *International Journal of Pharmacy and Biological Sciences*, **Vol.2(4), pp.168-172, 2012.**

[9] J. Podder, S. Ramalingom and S. Narayana Kalkura, "Crystallization and Characterization of Orthorhombic β -MgSO 4 ·7H 2 O Cryst," *Res. Technol*., **Vol.36(6), pp.549, 2001.**

[10] V. R. Raghorte, G. C. Wakde, N. S. Meshram and K. G. Rewatkar; "Harvesting amino acid doped KDP crystal by temperature and time control using AVR microcontroller,", *Results in Chemistry*, **Vol.2, pp.100074, 2020.**

[11] Akio Chiba, Tatzuo Ueki, Tamaichi Ashida, Yoshio Sasada and Masao Kakudo; "The crystal structure of L-ornithine hydrochloride," *Acta Crystallographica*. **Vol**, **22**, pp. **863-870,1967**

[12] Ferdousi Akhtar and Jiban Podar; "A Study on Structural, Optical, Electrical and Etching Characteristics of Pure and L-Alanine Doped Potassium Dihydrogen Phosphate Crystals," *Journal of Crystallization Process and Technology*, **Vol.1, pp.55, 2011.**

[13] B. Suresh Kumar and K. Rajendra Babu; "Effect of L-arginine, L-histidine and glycine on the growth of KDP single crystals and their characterization," *Indian Journal of Pure & Applied Physics*, **Vol.46, pp.123-126, 2008.**

[14] N. Pattanaboonmee, P. Ramasamy and P. Manyum; "Optical, thermal, dielectric and mechanical studies on glycine doped potassium dihydrogen orthophosphate singles crystals grown by SR method," *Proceedia Engineering*, **Vol.32, pp.1019-1025, 2012.**

[15] G. K. Williamson and W. H. Hall; "X-ray line broadening from filed aluminium and wolframL'elargissement des raies de rayons x obtenues des limailles d'aluminium et de tungsteneDie verbreiterung der roentgeninterferenzlinien von aluminium- und wolframspaenen," *Acta Metallurgica*, **Vol.1, pp.22-31, 1953.**

[16] C. N. J. Wagner and N. Haven; "Separation of particle size and lattice strain in integral breadth measurements," *Acta Crystallographica*, **Vol.20, pp.312-313, 1965.**

[17] C. N. J. Wagner and E. N. Aqua; **"**Analysis of the broadening of powder pattern peaks from cold-worked face-centered and body-centered cubic metals," *Advances in X-ray Analysis*, **Vol.7, pp.46-65, 1964.**

[18] M. Balaji, J. Chandrasekaran, M. Raja; "Role of substrate temperature on MoO3 thin films by the JNS pyrolysis technique for P–N junction diode application," *Materials Science in Semiconductor Processing*, **Vol.43, pp.104-113, 2016.**

[19] T. C. Paul, Jiban Podar; "Synthesis and characterization of Zn-incorporated TiO2 thin films: impact of crystallite size on X-ray line broadening and bandgap tuning," *Applied Physics A Materials Science & Processing*, **Vol.125, No.818, pp.1-14, 2019.**

[20] J. H. Joshi, G. M. Joshi, M. J. Joshi, H. O. Jethva, K. D. Parikh, "Raman, photoluminescence, and a.c. electrical studies of pure and l-serine doped ammonium dihydrogen phosphate single crystals: an understanding of defect chemistry in hydrogen bonding," *New Journal of Chemistry*., **Vol.42, pp.17227-17249, 2018.**

[21] G. Ramasamy, G. Bhagavannarayana and Subbiah Meenakshisundaram; "The concentration effects of s-, p-, d- and f-block element doping on the growth, crystalline perfection and properties of KDP crystals," *Cryst. Eng. Comm*., **Vol.14 3813-3819, 2012.**

[22] J. Tauc and A. Menth; *"*States in the gap," *Journal of Non-Crystalline Solids*, **Vol.8-10, pp.569-585, 1972.**

[23] M. A. Kaid and A. Ashour, "Preparation of ZnO-Doped Al Films by Spray Pyrolysis Technique," *Applied Surface Science*, **Vol**. **253**, No**. 6**, pp. **3029-3033, 2007.**

[24] J. H. Joshi, S. Kalainathan, D. K. Kanchan, M. J. Joshi, K. D. Parikh, "Effect of l-threonine on growth and properties of ammonium dihydrogen phosphate crystal," *Arabian Journal of Chemistry*., **Vol.13,** No. **1,** pp.**1532-1550, 2020.**

[25] M. Parthasarathy, M. Ananthraja, R. Gopalkrishnan; "Growth and characterization of large single crystals of l-serine methyl ester hydrochloride," *Journal of Crystal Growth*, **Vol.340, pp.118-122, 2012.**

[26] J. H. Joshi, K. P. Dixit, K. D. Parikh, H. O. Jethva, D. K. Kanchan, S. Kalainathan, M. J. Joshi, "Effect of Sr^{2+} on growth and properties of ammonium dihydrogen phosphate single crystal," *Journal of Materials Science: Materials in Electronics*., **Vol.29,** No.**7,** pp**.5837-5852, 2018.**

[27] A. Rawat, H. K. Mahavar, A. Tanwar, P. J. Singh; "Study of electrical properties of polyvinylpyrrolidone/polyacrylamide blend thin films," *Bulletin of Materials Science*, **Vol.37(2), pp.273-279, 2014.**

[28] F. Yakuphanoglu; "Electrical conductivity and electrical modulus properties of α, ω-dihexylsexithiophene organic semiconductor," *Physica B: Condensed Matter*, **Vol.393, Issue.1-2, pp.139-142, 2007.**

[29] A. Dutta, T. P. Sinha, P. Jena, S. Adak; "Ac conductivity and dielectric relaxation in ionically conducting soda–lime–silicate glasses," *Journal of Non-Crystalline Solids*, **Vol.354, pp.3952-3957, 2008.**

[30] S. B. Aziz, Z. H. Z. Abidin, A. K. Arof; "Influence of silver ion reduction on electrical modulus parameters of solid polymer electrolyte based on chitosan silver triflate electrolyte membrane," *eXPRESS Polymer Letters.,* **Vol.4(5), pp.300-310, 2010.**

[31] L. N. Patro, K. Hariharan; "AC conductivity and scaling studies of polycrystalline SnF2," *Materials Chemistry and Physics*., **Vol.116, pp.81-87, 2009.**

[32] P. G. R. Achary, Sonali Behera, R. N. P. Choudhary, S. K. Parida; "Retraction Note to: Structural, dielectric and electrical properties of cerium-modified strontium manganite ceramics," *Journal of Materials Science: Materials in Electronics*., **Vol.32, pp. 28944–28945, 2021.**

[33] N. K. Mohanty, S. K. Satapathy, B. Behera, P. Nayak, R. N. P. Choudhary; "Complex impedance properties of LiSr2Nb5O15 ceramic," *Journal of Advanced Ceramics*., **Vol.1, pp.221-226, 2012.**

[34] R. K. Parida, D. K. Pattanayak, B. N. Parida; "Impedance and modulus analysis of double perovskite Pb2BiVO6," *Journal of Materials Science: Materials in Electronics*, **Vol.28(22), pp. 16689-16695, 2017.**

[35] D. K. Pradhan, R. N. P. Choudhary, C. Rinaldi, R. S. Katiyar; "Effect of Mn substitution on electrical and magnetic properties of Bi0.9La0.1FeO3," *Journal of Applied Physics*., **Vol.106, pp.102, 2009.**

[36] M. J. Haun, E. Furman, S. J. Jang, L. E. Cross; "Thermodynamic theory of the lead zirconate-titanate solid solution system, part I: Phenomenology," *Ferroelectrics*, **Vol.99, pp.13, 1989.**

[37] I. Grinberg, V. R. Cooper, A. M. Rappe; "Oxide chemistry and local structure of PbZr x Ti 1 − x O 3 studied by density-functional theory supercell calculations," *PHYSICAL REVIEW B*, **Vol.69, pp.144118, 2004.**

[38] P. Kour, Pawan Kumar, S. K. Sinha, Manoranjan Kar; "Study of dielectric and impedance spectroscopy of La substituted nanocrystalline Pb(Zr0.52Ti0.48)O3 ceramics," *Journal of Materials Science: Materials in Electronics*, **Vol.26(3), pp.1304-1310, 2015.**

[39] A. Karmakar, S. Majumdar, S. Giri; "Polaron relaxation and hopping conductivity in LaMn 1 − x Fe x O 3," *PHYSICAL REVIEW B*, **Vol.79, pp.094406/1, 2009.**

[40] S. Bhattacharya, A. Gosh; "Conductivity relaxation in some fast ion-conducting AgI–Ag2O–V2O5 glasses," *Solid State Ionics*, **Vol.161, pp.61-65, 2003.**

[41] J. J. de Jonge, A. Van Zon, S. W. de Leeuw; "Molecular dynamics study of the influence of the polarizability in PEOx–NaI polymer electrolyte systems," *Solid State Ionics*, **Vol.147(3-4), pp.349-359, 2002.**

[42] Rajiv Ranjan, Nawnit Kumar, Banarji Behera, RNP Choudhary; "Investigations of impedance and electric modulus properties of Pb1-xSmx(Zr0.45 Ti0.55)1-x/4O3 ceramics," *ADVANCED MATERIALS Letters*, **Vol.5(3), pp.138-142, 2014.**

[43] R. J. Garhardt; "Impedance and dielectric spectroscopy revisited: Distinguishing localized relaxation from long-range conductivity," *Journal of Physics and Chemistry of Solids*, **Vol.55, No.12, pp.1491-1506, 1994.**

[44] D. Shyamala, R. Rathikha, K. Gomathi; "Dielectric Investigation on Single Crystals of Morpholium Cadmium Aceto-perchlorate," *International Journal of Pure and Applied Physics*., **Vol.12(1), pp.35-46, 2016.**

[45] J. H. Joshi, D. K. Kanchan, M. J. Joshi, H. O. Jethva, K. D. Parikh, "Dielectric Relaxation, Complex Impedance and Modulus Spectroscopic Studies of Mix Phase Rod Like Cobalt Sulfide Nanoparticles," *Materials Research Bulletin.,* **Vol.93, pp.63-73, 2017.**

[46] J. C. Anderson; "Dielectrics," *Chapman and Hall*, **London, p.16, 1964.**

[47] A. J. Moulson, J. M. Herbert; "Electroceramics: Materials, Properties and Applications," *Chapman & Hall*, **London, 1990.**

[48] E. E. Shaisha, F. El-Desouki Sh, I. Shaltout, A. A. Bahgat; "Electrical Relaxation in Mixed Alkali Bi2O3-K2O-Li2O-Fe2O3 Glasses," *J. Mater. Sci. Technol*., **Vol.22, pp.701-707, 2006.**

[49] U. Ahmadu, S. Tomas, S. A. Jonah, A. O. Musa, N. Rabiu; "Equivalent circuit models and analysis of impedance spectra of solid electrolyte Na0.25Li0.75Zr2(PO4)3," *Advanced Materials Letters*, **Vol.4(3), pp.185-195, 2013.**

[50] Benjamin D. Hatton, Kai Landskron, William J. Hunks, Mark R. Bennett, Donna Shukaris, Douglas D. Perovic, Geoffrey A. Ozin; "Materials chemistry for low-k materials," *Materials Today*, **Vol.9(3), pp.22-31, 2006.**

[51] M. P. Dasari, K. Sambasiva Rao, P. Murali Krishna, G. Gopala Krishna; "Barium Strontium Bismuth Niobate Layered Perovskites: Dielectric, Impedance and Electrical Modulus Characteristics," *Acta Physica Polonica A*, **Vol.119(3), pp.387-394, 2011.**

[52] R. Gao, Q. Zhang, Z. Xu, Z. Wang, C. Fu, G. Chen, X. Deng, W. Cai; "A comparative study on the structural, dielectric and multiferroic properties of Co0.6Cu0.3Zn0.1Fe2O4/Ba0.9Sr0.1Zr0.1Ti0.9O3 composite ceramics," *Composites Part B: Engineering*, **Vol.166, pp.204, 2019.**

[53] R. Gao, X, Qin, Q. Zhang, Z. Xu, Z. Wang, C. Fu, G. Chen, X. Deng, W. Cai; "Enhancement of magnetoelectric properties of (1-x)Mn0.5Zn0.5Fe2O4-xBa0.85Sr0.15Ti0.9Hf0.1O3 composite ceramics," *Journal of Alloys and Compounds*, **Vol.795, pp.501-512, 2019.**

[54] R. Tripathi, A. Kumar, T. P. Sinha; "Dielectric properties of CdS nanoparticles synthesized by soft chemical route," *Pramana – Journal of Physics - J Phys*., **Vol.72, pp.969, 2009.**

[55] Khushbu Gohel, D. K. Kanchan; "Ionic conductivity and relaxation studies in PVDF-HFP:PMMA-based gel polymer blend electrolyte with LiClO4 salt," *Journal of Advanced Dielectrics,* **Vol.8, pp. 1850005-1, 2018.**

[56] R. M. Hill, A. K. Jonscher; "DC and AC conductivity in hopping electronic systems," *J. Non-Cryst. Solids*, **Vol.32, pp.53-69, 1979.**

[57] A. R. Long, M. Pollak, B. I. Shklovskii; "Hopping Transport in Solids," *Elsevier Science Publishers*, **Netherlands, pp.207, 1991.**

[58] A. G. Hunt; "Ac hopping conduction: Perspective from percolation theory," *Philosophical Magazine B*, **Vol.81, pp.875-913, 2001.**

[59] L. Thansanga, Alok Shukla, Nitin Kumar, R. N. P. Choudhary; "Studies of structural, dielectric and electrical characteristics of Bi(Fe0.85Y0.15)O3 ceramics," *Phase Transitions*, **Vol.94(1), pp.47-61, 2021.**

[60] K. Sambasiva Rao, P. Murali Krishna, D. Madhava Prasad, T. Swana Latha, C. Satyanarayana; "Low frequency dielectric dispersion studies in ferroelectric ceramics of $Pb_{0.77}K_{0.26}Li_{0.2}Ti_{0.25}Nb_{1.8}O_6$," *Indian J. Eng. Mater. Sci*., **Vol.15, pp.215-223, 2008.**

[61] S. R. Elliot; "A.c. conduction in amorphous chalcogenide and pnictide semiconductors," *Advances in Physics*., **Vol.36(2), pp.135-217, 1987.**

[62] Funke; "Jump relaxation in solid electrolytes," *Progress in Solid State Chemistry*, **Vol.22 (2), pp.111-195, 1993.**

[63] S. Upadhyaya, S. Kumar, D. Ashok Kumar, Om Prakash; "Probing electrical conduction behavior of BaSnO3," *Journal of Applied Physics*, **Vol.84(2), pp.828, 1998.**

[64] S. Sen, R. N. P. Choudhary; "Impedance studies of Sr modified BaZr0. 05Ti0. 95O3 ceramics," *Materials Chemistry and Physics*, **Vol.87, pp.256-263, 2004.**

[65] T. R. Shrout, L. E. Cross, D. A. Hukin; "Ferroelectric properties of tungsten bronze lead barium niobate (PBN) single crystals," Ferroelectric., **Vol.44, pp.325-330, 1983.**

[66] Bilal Hamid Bhat, Rubiya Samad, Basharat Want; "Dielectric and impedance behavior of neodymium substituted strontium hexaferrite," *Applied Physics A*, **Vol.122, No. 810, pp.1-11, 2016.**

[67] N.H. Manani, H.O. Jethva, M.J. Joshi; "Dielectric Relaxation, Conductivity Mechanism and Complex Impedance Spectroscopic Studies of Pure and Cadmium Mixed Cobalt Levo-Tartrate Crystals," *IJSRPAS*, **Vol.8**, **Issue.1, pp.8-15, 2020.**

[68] K. A. Mauritz; "Dielectric relaxation studies of ion motions in electrolyte-containing perfluorosulfonate ionomers. 4. Long-range ion transport," *Macromolecules*, **Vol.22, pp.4483-4488, 1989.**

[69] S. R. Elliott, A. P. Owens; "The diffusion controlled relaxation model for ionic transport in glasses," *Philos. Magn*., **Vol.60(6), pp.777-792, 1989.**

[70] B. S. Kamble1, V. J. Fulari, R. K. Nimat; "A. C. Conductivity and Dielectric Study of Strontium Doped Lanthanum Manganite (LSM) thin films as Cathode for SOFC," *IJSRPAS*, **Vol.6**, **Issue.5, pp.115-117, 2018.**

[71] B. K. Chaudhuri, K. Chaudhuri, K. K. Som, "Concentration and frequency dependences of ac conductivity and dielectric constant of Iron-Bismuth oxide glasses," *J. Phys. Chem. Solids*, **Vol.50**, **Issue.11, pp.1149-1155, 1989.**

[72] L. B. Harris, G. J. Vella; "Conductivity of Single Crystals of Potassium Dihydrogen Phosphate," *Journal of Applied Physics*., **Vol.37(11), pp.4294, 1967.**

[73] J. H. Joshi, D. K. Kanchan, H. O. Jethva, M. J. Joshi, K. D. Parikh; "Dielectric relaxation, protonic defect, conductivity mechanisms, complex impedance and modulus spectroscopic studies of pure and L-threonine-doped ammonium dihydrogen phosphate," *Ionics*, **Vol.24(7), pp.1995-2016, 2018.**

